Study on Multiscale Hydrodynamic Step Bearing

Shaojing Shao, Yongbin Zhang*, Xuedong Jiang and Pingjun Pang

College of Mechanical Engineering, Changzhou University, Changzhou, Jiangsu Province, China

Abstract: In a step bearing, when the surface separation is so low that it is comparable with the thickness of the physical adsorbed layer on the bearing surface, the physical adsorbed layer should have an influence on the bearing performance. The present paper presents a multiscale analysis for this multiscale hydrodynamic bearing by considering the effect of the adsorbed layer but neglecting the interfacial slippage on any interface. The adsorbed layer flow is described by the nanoscale flow equation, and the intermediate continuum fluid flow is simulated based on the Newtonian fluid model. The pressure distribution and carried load of the bearing were derived. Exemplary calculations show that when the surface separation in the bearing outlet zone is below 100nm but no less than 10nm, for a weak fluid-bearing surface interaction both the pressure and carried load of the bearing are just slightly higher than those calculated from the conventional hydrodynamic lubrication theory, for a medium fluid-bearing surface interaction the differences are further enlarged, and for a strong fluid-bearing surface interaction the differences are mostly enlarged. The results show the very significant multiscale effect in this bearing resulting in the pronounced improvement of the load-carrying capacity of the bearing by the medium and strong fluid-bearing surface interactions when the surface separation in the bearing outlet zone is below 100nm.

Keywords: Adsorbed layer, Bearing, Hydrodynamics, Load, Multiscale, Pressure.

1. INTRODUCTION

Conventional hydrodynamic lubrication theories have been established long time [1]. They have been used for designing hydrodynamic lubricated thrust and journal bearings. They take the fluid as continuum and ignore the fluid-bearing surface interaction effect, which may be significant for low bearing surface separations. It is familiar that those theories can be successful for relatively high surface separations. However, for very low surface separations such as below 50nm, Chan and Horn [2] found that conventional continuum lubrication theory failed for the drainage force experiment in a mica surface contact. They observed the unexpected high drainage forces. They suggested that for such cases the effect of the boundary layer physically adhering to the contact surface should not be neglected. They found that it was successful to predict the experimental observation by assuming a molecular scale solid layer on the surface and calculating the equivalent viscosity of the continuum fluid intervening between the two solid layers.

Because of the fluid-solid surface interaction, there is an adhering layer on the solid surface with the thickness of several molecule diameters [2, 3]. Both the average density and effective viscosity of the layer are normally considerably increased compared to the bulk fluid values [2-5]. By the entrainment of the solid surface or the pressure driving, there is the layer flow, which is on the molecular scale and distinctly different from the conventional fluid flow. When the surface separation is so low that it is comparable with the thickness of the adsorbed layer, the layer flow rate may be comparable to or even greater than the flow rate of the intermediate continuum fluid. In this case, the adsorbed layer effect should be significant and can not be neglected.

It is obvious that conventional hydrodynamic lubrication theories are insufficient for critically low lubricating film thicknesses owing to neglecting the effect of the adsorbed layer on the solid surface. Currently, there are no theories developed for this low film thickness range for describing the performances of hydrodynamic lubricated bearings. The present study aims to undertake this work by addressing a hydrodynamic step bearing with low surface separations.

2. MULTISCALE HYDRODYNAMIC STEP BEARING

The multiscale hydrodynamic step bearing with a normal geometrical configuration is shown in Figure **1**. The bearing length is assumed as sufficiently large so that the side leakage effect in the bearing is negligible. In this bearing, the surface separation is so low that it is comparable with the thickness h_{bf} of the adsorbed layer on the bearing surface; Between the two adsorbed layers is the continuum fluid flow, which is here assumed as Newtonian. In the present study, the adsorbed layers on the two bearing surfaces are assumed as identical; The fluid-bearing surface interaction may be weak, medium and strong.

*Address correspondence to this author at the College of Mechanical Engineering, Changzhou University, Changzhou, Jiangsu Province, China; Tel: 86+519+86550562; E-mail: engmech1@sina.com

E-ISSN: 2409-9848/20

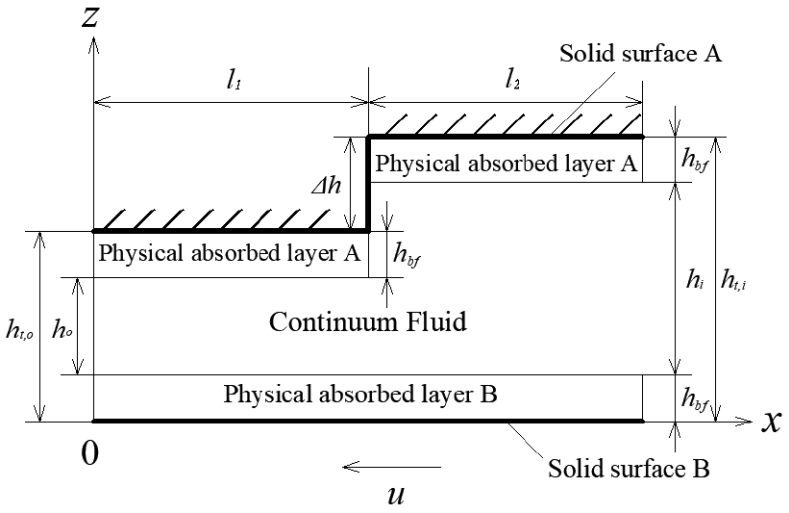

Figure 1: The studied multiscale hydrodynamic step bearing.

The upper bearing surface is stationary, and the lower bearing surface is moving with the speed u. The widths of the inlet and outlet zones of the bearing are respectively l_2 and l_1, and the bearing step size is Δh. The surface separations in the inlet and outlet zones are respectively $h_{t,i}$ and $h_{t,o}$, and the continuum fluid film thicknesses in these two zones are respectively h_i and h_o. The used coordinates are also shown in Figure **1**.

3. ANALYSIS

The flow of physical adsorbed layer can be modeled by molecular dynamics simulation [6-10]. However, it normally takes an unaffordable time for an engineering problem. Here, the adsorbed layer flow is simulated by the flow factor approach model [11], which was developed for nanoscale flow. The flow of the intermediate continuum fluid is simulated by the Newtonian fluid model. The detailed analysis for the multiscale flow in the bearing in Figure **1** based on the simulation approaches has been shown in Ref.12. The analysis is based on the following assumptions: (a) The fluid inertia is negligible; (b) The flow is isothermal; (c) The flow is in laminar flow; (d) The influences of the fluid pressure on both the fluid density and the fluid viscosity are negligible (e) The interfacial slippage effect on any interface is neglected. These assumptions are particularly allowable for the operating condition of light loads and low sliding speeds.

3.1. For the Inlet Zone

In this sub-zone, the total mass flow rate per unit contact length through the bearing is [12]:

$$q_m = -uh_{bf}\rho_{bf}^{eff} - \frac{uh_i}{2}\rho - \frac{h_i^3\rho}{12\eta}\frac{\partial p}{\partial x} + \frac{h_{bf}^3\rho_{bf}^{eff}}{\eta_{bf}^{eff}}\frac{\partial p}{\partial x}\left[\frac{F_1}{6} - \frac{\varepsilon}{1+\frac{\Delta x}{D}}\left(1+\frac{1}{2\lambda_{bf,i}} - \frac{q_0-q_0^n}{q_0^{n-1}-q_0^n}\frac{\Delta_{n-2}}{h_{bf}}\right)\right] + \frac{h_i^3\rho}{\eta_{bf}^{eff}}\frac{\partial p}{\partial x}\left[\frac{F_2\lambda_{bf,i}^2}{6} - \frac{\lambda_{bf,i}}{1+\frac{\Delta x}{D}}\left(\frac{1}{2}+\lambda_{bf,i} - \frac{q_0-q_0^n}{q_0^{n-1}-q_0^n}\frac{\Delta_{n-2}}{h_i}\right)\right] \quad (1)$$

where $\lambda_{bf,i} = h_{bf}/h_i$, u is positive, p is the fluid film pressure, and η are respectively the bulk density and bulk viscosity of the fluid, ρ_{bf}^{eff} and η_{bf}^{eff} are respectively the average density and the effective viscosity of the physical adsorbed layer, *D* and Δx are respectively the fluid molecule diameter and the separation between the neighboring fluid molecules in the *x* coordinate direction in the adsorbed layer, $q_0 = \Delta_{j+1}/\Delta_j$ (Δ_j is the separation between the (*j+1*)th and *j*th fluid molecules across the layer thickness) and q_0 is constant, $\varepsilon = (2DI + II)/[h_{bf}(n-1)(\Delta_l/\eta_{line,l})_{avr,n-1}]$, $F_1 = \eta_{bf}^{eff}(12D^2\Psi + 6D\Phi)/h_{bf}^3$, n is the equivalent number of the fluid molecules across the layer thickness, and Δ_{n-2} is the separation between the neighboring fluid molecules across the layer thickness just on the adsorbed layer-fluid interface. Here,

$$I = \sum_{i=1}^{n-1} i(\Delta_l/\eta_{line,l})_{avr,i}, \qquad \Psi = \sum_{i=1}^{n-1} i(l\Delta_{l-1}/\eta_{line,l-1})_{avr,i},$$

$$II = \sum_{i=0}^{n-2}[i(\Delta_l/\eta_{line,l})_{avr,i} + (i+1)(\Delta_l/\eta_{line,l})_{avr,i+1}]\Delta_i,$$

$\Phi = \sum_{i=0}^{n-2} [\, i(l\Delta_{l-1} / \eta_{line,l-1})_{avr,i} + (i+1)(l\Delta_{l-1} / \eta_{line,l-1})_{avr,i+1}]\Delta_i$,

$i(\Delta_l / \eta_{line,l})_{avr,i} = \sum_{j=1}^{i} \Delta_{j-1} / \eta_{line,j-1}$, and

$i(l\Delta_{l-1} / \eta_{line,l-1})_{avr,i} = \sum_{j=1}^{i} j\Delta_{j-1} / \eta_{line,j-1}$; $\eta_{line,j-1}$ is the local viscosity between the j^{th} and $(j\text{-}1)^{th}$ fluid molecules across the layer thickness, and $\eta_{line,j} / \eta_{line,j+1} = q_0^{\gamma}$.

Integrating Eq. (1) gives that:

$$p(x) = \frac{\left(q_m + uh_{bf}\rho_{bf}^{eff} + \frac{uh_i}{2}\rho \right)x + c_1}{A_1} \tag{2}$$

where c_1 is an integral constant and

$$A_1 = -\frac{h_i^3\rho}{12\eta} + \frac{h_{bf}^3\rho_{bf}^{eff}}{\eta_{bf}^{eff}}\left[\frac{F_1}{6} - \frac{\varepsilon}{1+\frac{\Delta x}{D}}\left(1 + \frac{1}{2\lambda_{bf,i}} - \frac{q_0 - q_0^n}{q_0^{n-1} - q_0^n}\frac{\Delta_{n-2}}{h_{bf}} \right) \right] + \frac{h_i^3\rho}{\eta_{bf}^{eff}}\left[\frac{F_2\lambda_{bf,i}^2}{6} - \frac{\lambda_{bf,i}}{1+\frac{\Delta x}{D}}\left(\frac{1}{2} + \lambda_{bf,i} - \frac{q_0 - q_0^n}{q_0^{n-1} - q_0^n}\frac{\Delta_{n-2}}{h_i} \right) \right] \tag{3}$$

Based on the boundary condition $p|_{x=l_1+l_2} = 0$, it is solved from Eq.(2) that:

$$c_1 = -(l_1 + l_2)\left(q_m + uh_{bf}\rho_{bf}^{eff} + \frac{uh_i}{2}\rho \right) \tag{4}$$

The pressure in the inlet zone is thus:

$$p(x) = F_{1,i}(x)\cdot q_m + F_{2,i}(x), \qquad \text{for } l_1 \le x \le l_1 + l_2 \tag{5}$$

where

$$F_{1,i}(x) = \frac{x - (l_1 + l_2)}{A_1} \tag{6}$$

and

$$F_{2,i}(x) = \frac{x - (l_1 + l_2)}{A_1}\left(uh_{bf}\rho_{bf}^{eff} + \frac{uh_i}{2}\rho \right) \tag{7}$$

Equation (5) gives the pressure on the boundary between the inlet and outlet zones as:

$$p|_{x=l_1} = F_{1,i}(l_1)\cdot q_m + F_{2,i}(l_1) \tag{8}$$

3.2. For the Outlet Zone

In this sub-zone, the total mass flow rate per unit contact length through the bearing is [12]:

$$q_m = -uh_{bf}\rho_{bf}^{eff} - \frac{uh_o}{2}\rho - \frac{h_o^3\rho}{12\eta}\frac{\partial p}{\partial x} + \frac{h_{bf}^3\rho_{bf}^{eff}}{\eta_{bf}^{eff}}\frac{\partial p}{\partial x}\left[\frac{F_1}{6} - \frac{\varepsilon}{1+\frac{\Delta x}{D}}\left(1 + \frac{1}{2\lambda_{bf,o}} - \frac{q_0 - q_0^n}{q_0^{n-1} - q_0^n}\frac{\Delta_{n-2}}{h_{bf}} \right) \right] + \frac{h_o^3\rho}{\eta_{bf}^{eff}}\frac{\partial p}{\partial x}\left[\frac{F_2\lambda_{bf,o}^2}{6} - \frac{\lambda_{bf,o}}{1+\frac{\Delta x}{D}}\left(\frac{1}{2} + \lambda_{bf,o} - \frac{q_0 - q_0^n}{q_0^{n-1} - q_0^n}\frac{\Delta_{n-2}}{h_o} \right) \right] \tag{9}$$

where $\lambda_{bf,o} = h_{bf} / h_o$.

In the conventional bearing condition, the bearing surface separation h_o in the outlet zone is far greater than the thickness h_{bf} of the adsorbed layer so that the flow of the adsorbed layer in the whole bearing is negligible and also both the values of $\lambda_{bf,o}$ and $\lambda_{bf,i}$ approach to vanishing. For this condition, equations (1) and (9) reduce to the conventional Reynolds equation [1] for hydrodynamic lubrication, and the present calculation results are the same with those calculated from conventional hydrodynamic lubrication theory.

Integrating Eq. (9) gives that:

$$p(x) = \frac{\left(q_m + uh_{bf}\rho_{bf}^{eff} + \frac{uh_o}{2}\rho \right)x + c_2}{A_2} \tag{10}$$

where c_2 is an integral constant and

$$A_2 = -\frac{h_o^3\rho}{12\eta} + \frac{h_{bf}^3\rho_{bf}^{eff}}{\eta_{bf}^{eff}}\left[\frac{F_1}{6} - \frac{\varepsilon}{1+\frac{\Delta x}{D}}\left(1 + \frac{1}{2\lambda_{bf,o}} - \frac{q_0 - q_0^n}{q_0^{n-1} - q_0^n}\frac{\Delta_{n-2}}{h_{bf}} \right) \right] + \frac{h_o^3\rho}{\eta_{bf}^{eff}}\left[\frac{F_2\lambda_{bf,o}^2}{6} - \frac{\lambda_{bf,o}}{1+\frac{\Delta x}{D}}\left(\frac{1}{2} + \lambda_{bf,o} - \frac{q_0 - q_0^n}{q_0^{n-1} - q_0^n}\frac{\Delta_{n-2}}{h_o} \right) \right] \tag{11}$$

Based on the boundary condition $p|_{x=0} = 0$, it is solved from Eq.(10) that $c_2 = 0$. The pressure in the outlet zone is thus:

$$p(x) = F_{1,o}(x)\cdot q_m + F_{2,o}(x), \qquad \text{for } 0 \le x \le l_1 \tag{12}$$

where

$$F_{1,o}(x)=\frac{x}{A_2} \tag{13}$$

and

$$F_{2,o}(x)=\frac{x}{A_2}\left(uh_{bf}\rho_{bf}^{eff}+\frac{uh_o}{2}\rho\right) \tag{14}$$

Equation (13) gives the pressure on the boundary between the inlet and outlet zones as:

$$p|_{x=l_1}=F_{1,o}(l_1)\cdot q_m+F_{2,o}(l_1) \tag{15}$$

3.3. Mass Flow Rate and Carried Load of the Bearing

Solving the coupled equations (8) and (15) gives the mass flow rate per unit contact length through the bearing as:

$$q_m=\frac{F_{2,o}(l_1)-F_{2,i}(l_1)}{F_{1,i}(l_1)-F_{1,o}(l_1)} \tag{16}$$

The load per unit contact length carried by the bearing is:

$$\begin{aligned}w&=\int_0^{l_1+l_2}p\,dx\\&=q_m\int_0^{l_1}F_{1,o}(x)\,dx+\int_0^{l_1}F_{2,o}(x)\,dx+q_m\int_{l_1}^{l_1+l_2}F_{1,i}(x)\,dx+\int_{l_1}^{l_1+l_2}F_{2,i}(x)\,dx\\&=\frac{q_m l_1^2}{2A_2}+\frac{l_1^2}{2A_2}\left(uh_{bf}\rho_{bf}^{eff}+\frac{uh_o}{2}\rho\right)-\frac{q_m l_2^2}{2A_1}-\frac{l_2^2}{2A_1}\left(uh_{bf}\rho_{bf}^{eff}+\frac{uh_i}{2}\rho\right)\end{aligned} \tag{17}$$

3.4. Normalization

For generality, the results have been normalized and the following dimensionless parameters are used:

$$\psi=\frac{l_1}{l_2},\quad X=\frac{x}{l_1+l_2},\quad \alpha=\frac{h_o}{l_1+l_2},\quad K=\frac{1}{\alpha},\quad r=\frac{h_i}{h_o}=1+\frac{\Delta h}{h_o},$$

$$P=\frac{ph_{t,o}}{u\eta_a},\quad W=\frac{w}{u\eta_a},\quad Q_m=\frac{q_m}{uh_o\rho_a},\quad H_{bf}=\frac{h_{bf}}{h_{cr,bf}},\quad Cq=\frac{\rho_{bf}^{eff}}{\rho_a},$$

$$Cy=\frac{\eta_{bf}^{eff}}{\eta_a},\quad \overline{F}_{1,i}=\frac{F_{1,i}\rho_a h_i^2}{\eta_a},\quad \overline{F}_{2,i}=\frac{F_{2,i}h_i}{u\eta_a},\quad \overline{F}_{1,o}=\frac{F_{1,o}\rho_a h_o^2}{\eta_a},$$

$$\overline{F}_{2,o}=\frac{F_{2,o}h_o}{u\eta_a}$$

Here, ρ_a and η_a are respectively the bulk density and the bulk viscosity of the fluid at ambient condition, and $h_{cr,bf}$ is the critical film thicknesses.

3.4.1. For the Present Multiscale Analysis

Thus, $\overline{F}_{1,i}$, $\overline{F}_{2,i}$, $\overline{F}_{1,o}$ and $\overline{F}_{2,o}$ are respectively:

$$\overline{F}_{1,i}(X)=\frac{K(X-1)}{rB_1} \tag{18}$$

$$\overline{F}_{2,i}(X)=\frac{K(X-1)}{rB_1}\left(\lambda_{bf,i}Cq+\frac{1}{2}\right) \tag{19}$$

$$\overline{F}_{1,o}(X)=\frac{KX}{B_2} \tag{20}$$

$$\overline{F}_{2,o}(X)=\frac{KX}{B_2}\left(\lambda_{bf,o}Cq+\frac{1}{2}\right) \tag{21}$$

where

$$B_1=-\frac{1}{12}+\frac{Cq\lambda_{bf,i}^3}{Cy}\left[\frac{F_1}{6}-\frac{\varepsilon}{1+\frac{\Delta x}{D}}\left(1+\frac{1}{2\lambda_{bf,i}}-\frac{q_0-q_0^n}{q_0^{n-1}-q_0^n}\frac{\Delta_{n-2}}{h_{bf}}\right)\right]$$
$$+\frac{1}{Cy}\left[\frac{F_2\lambda_{bf,i}^2}{6}-\frac{\lambda_{bf,i}}{1+\frac{\Delta x}{D}}\left(\frac{1}{2}+\lambda_{bf,i}-\frac{q_0-q_0^n}{q_0^{n-1}-q_0^n}\frac{\Delta_{n-2}\lambda_{bf,i}}{h_{bf}}\right)\right] \tag{22}$$

$$B_2=-\frac{1}{12}+\frac{Cq\lambda_{bf,o}^3}{Cy}\left[\frac{F_1}{6}-\frac{\varepsilon}{1+\frac{\Delta x}{D}}\left(1+\frac{1}{2\lambda_{bf,o}}-\frac{q_0-q_0^n}{q_0^{n-1}-q_0^n}\frac{\Delta_{n-2}}{h_{bf}}\right)\right]$$
$$+\frac{1}{Cy}\left[\frac{F_2\lambda_{bf,o}^2}{6}-\frac{\lambda_{bf,o}}{1+\frac{\Delta x}{D}}\left(\frac{1}{2}+\lambda_{bf,o}-\frac{q_0-q_0^n}{q_0^{n-1}-q_0^n}\frac{\Delta_{n-2}\lambda_{bf,o}}{h_{bf}}\right)\right] \tag{23}$$

The dimensionless mass flow rate per unit contact length through the bearing is:

$$Q_m=\frac{r^2\overline{F}_{2,o}-r\overline{F}_{2,i}}{\overline{F}_{1,i}-r^2\overline{F}_{1,o}} \tag{24}$$

The dimensionless pressure in the inlet zone is:

$$P(X)=\frac{Q_m}{r^2}\overline{F}_{1,i}(X)+\frac{\overline{F}_{2,i}(X)}{r},\ \text{for}\ \frac{\psi}{\psi+1}\le X\le 1 \tag{25}$$

The dimensionless pressure in the outlet zone is:

$$P(X)=Q_m\overline{F}_{1,o}(X)+\overline{F}_{2,o}(X),\ \text{for}\ 0\le X\le\frac{\psi}{\psi+1} \tag{26}$$

The dimensionless load carried by the bearing is:

$$W=\frac{K^2Q_m}{2A_2}\left(\frac{\psi}{\psi+1}\right)^2+\frac{K^2}{2A_2}\left(\lambda_{bf,o}Cq+\frac{1}{2}\right)\left(\frac{\psi}{\psi+1}\right)^2 -\frac{K^2Q_m}{2r^3A_1}\left(\frac{1}{\psi+1}\right)^2-\frac{K^2}{2r^2A_1}\left(\lambda_{bf,i}Cq+\frac{1}{2}\right)\left(\frac{1}{\psi+1}\right)^2 \tag{27}$$

3.4.2. For the Conventional Hydrodynamic Theory

For comparison, the results for the bearing in Figure **1** calculated from the conventional hydrodynamic theory [1] are presented in this section.

The dimensionless hydrodynamic film pressure in the bearing is:

$$P(X)=K(1-X)\left(\frac{6}{r^2}+\frac{12Q_m}{r^3}\right),\ \text{for}\ \frac{\psi}{\psi+1}\le X\le 1 \tag{28}$$

and

$$P(X)=-KX(6+12Q_m),\ \text{for}\ 0\le X\le\frac{\psi}{\psi+1} \tag{29}$$

where

$$Q_m=-\frac{\psi r^3+r}{2\psi r^3+2} \tag{30}$$

The dimensionless carried load by the bearing is:

$$W=\left(\frac{1}{\psi+1}\right)^2\left(\frac{3K^2}{r^2}+\frac{6Q_mK^2}{r^3}\right)-\left(\frac{\psi}{\psi+1}\right)^2\left(3K^2+6Q_mK^2\right) \tag{31}$$

4. CALCULATION

In the calculation, it was taken that $\Delta_{n-2}/D=0.15$, $D=0.5$ and l_1+l_2 =2×10^{4}nm. The parameter Cq is expressed as[13]:

$$Cq(H_{bf})=\begin{cases}1 & ,\quad \text{for}\ H_{bf}\ge 1\\ m_0+m_1H_{bf}+m_2{H_{bf}}^2+m_3{H_{bf}}^3 & ,\quad \text{for}\ 0<H_{bf}\le 1\end{cases} \tag{32}$$

where $m_o, m_1, m_2\ and\ m_3$ are respectively constant.

The parameter Cy is expressed as[13]:

$$Cy(H_{bf})=\begin{cases}1 & ,\quad \text{for}\ H_{bf}\ge 1\\ a_0+a_1/H_{bf}+a_2/{H_{bf}}^2 & ,\quad \text{for}\ 0<H_{bf}\le 1\end{cases} \tag{33}$$

where a_o, a_1 and a_2 are respectively constant.

F_1, F_2 and ε are respectively regressed out as[13]:

$$F_1=0.18\left(\Delta_{n-2}/D-1.905\right)\left(\ln n-7.897\right) \tag{34}$$

$$F_2=-3.707\times10^{-4}\left(\Delta_{n-2}/D-1.99\right)\left(n+64\right)\left(q_0+0.19\right)\left(\gamma+42.43\right) \tag{35}$$

$$\varepsilon=4.56\times10^{-6}\left(\Delta_{n-2}/D+31.419\right)\left(n+133.8\right)\left(q_0+0.188\right)\left(\gamma+41.62\right) \tag{36}$$

The weak, medium and strong fluid-bearing surface interactions were respectively used. For the weak interaction: $h_{cr,bf}$ =7nm, γ =0.5, *n*=3, q_o =1.05; For the medium interaction: $h_{cr,bf}$ =20nm, γ =1.0, *n*=5, q_o =1.1; For the strong interaction: $h_{cr,bf}$ =40nm, γ =1.5, *n*=8, q_0 =1.2. For these three interactions, the viscosity and density parameter values are respectively shown in Tables **1a** and **b**. For the weak, medium and strong fluid-bearing surface interactions, the thicknesses of the adsorbed layer are respectively 1.65nm, 2.76nm and 4.32nm.

Table 1a: Fluid Viscosity Data for Different Fluid-Bearing Surface Interactions [13]

Parameter / Interaction	a_0	a_1	a_2
Strong	1.8335	-1.4252	0.5917
Medium	1.0822	-0.1758	0.0936
Week	0.9507	0.0492	1.6447×10^{-4}

Table 1b: Fluid Density Data for Different Fluid-Bearing Surface Interactions [13]

Parameter / Interaction	m_0	m_1	m_2	m_3
Strong	1.43	-1.723	2.641	-1.347
Medium	1.30	-1.065	1.336	-0.571
Week	1.116	-0.328	0.253	-0.041

5. RESULTS

5.1. Pressure Distribution

For Δh=4nm and ψ=1, Figures **2**(**a**)-(**d**) respectively show the dimensionless hydrodynamic film pressures in the bearing for the weak, medium and strong fluid-bearing surface interactions and calculated from the conventional hydrodynamic theory when $h_{t,o}$=10nm, 20nm, 30nm and 40nm. The film pressures for the weak fluid-bearing surface interaction are just slightly higher than those calculated from the conventional hydrodynamic theory for the film thickness range. For $h_{t,o}$=10nm, the film pressures for the medium fluid-bearing surface interaction are much greater than those calculated from the conventional hydrodynamic theory, while those for the strong fluid-bearing surface interaction are far greater than those calculated from the conventional hydrodynamic theory. These show the very significant multiscale effect in the bearing and the significant influence of the fluid-bearing surface interaction on the film pressure by the adsorbed layer when the bearing surface separation is on the same scale with the thickness of the adsorbed layer. For the strong fluid-bearing surface interaction, the adsorbed layer is heavily solidified, it is equivalent to significantly reduce the surface separation of the bearing, so the film pressure in the bearing is largely increased. For the weak fluid-bearing surface interaction, the adsorbed layer flows well, and its effect on the film pressure is not obvious. The increase of $h_{t,o}$ appears to alleviate the adsorbed layer effect and results in the film pressures closer to the conventional ones for any fluid-bearing surface interaction.

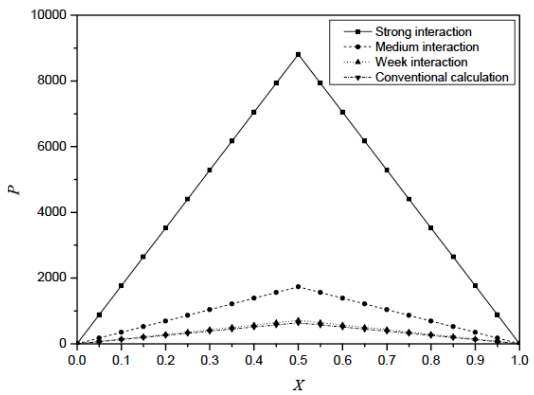

(**a**) $h_{t,o}$=10nm

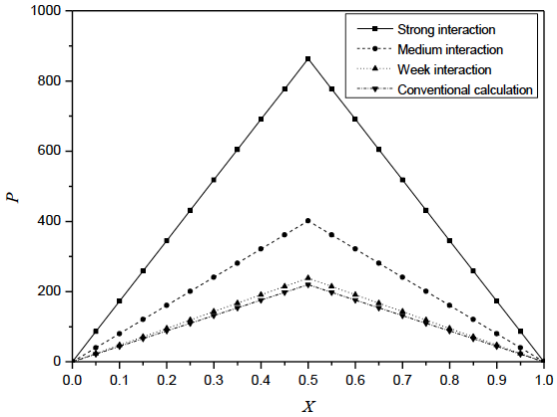

(**b**) $h_{t,o}$=20nm

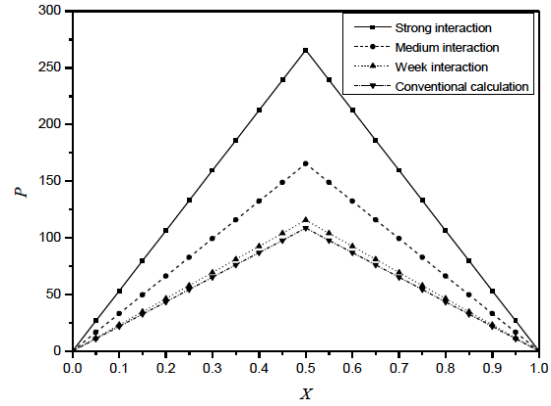

(**c**) $h_{t,o}$=30nm

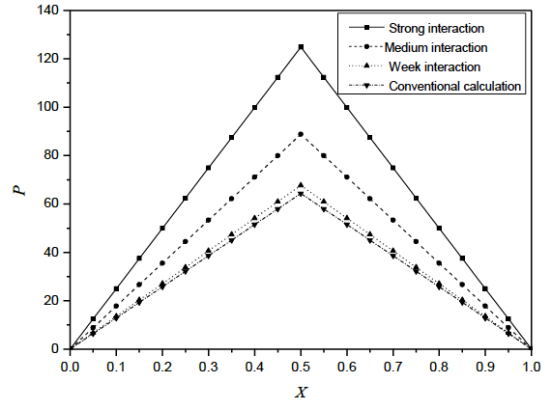

(**d**) $h_{t,o}$=40nm

Figure 2: Dimensionless pressure distributions in the bearing at different two solid surface clearance thicknesses, when Δh=4nm, ψ=1, $l_1 + l_2$=2×10^{4}nm

5.2. Carried Load of the Bearing

Figure **3** shows the variations with the outlet surface separation $h_{t,o}$ of the dimensionless loads carried by the bearing respectively for the weak, medium and strong fluid-bearing surface interactions and calculated from the conventional hydrodynamic teory when Δh=4nm and ψ=1. For $h_{t,o} \leq 100nm$, the multiscale effect is very significant for both the medium and strong interaction types and it greatly increases the load-carrying capacity of the bearing especially when $h_{t,o}$ is low. This indicates the correspondingly very significant effect of the adsorbed layer, but strongly suggests that we still can not conclude that the bearing has entered into the non-continuum lubrication regime according to the observation as there is a quite thick continuum fluid film between the two adsorbed layers. The over high load-carrying capacity is just because of the multiscale effect in the bearing. For the weak fluid-bearing surface interaction, the adsorbed layer effect is negligible and the carried loads of the bearing are just a little higher than those calculated from the conventional hydrodynamic theory when $h_{t,o} \geq 10nm$.

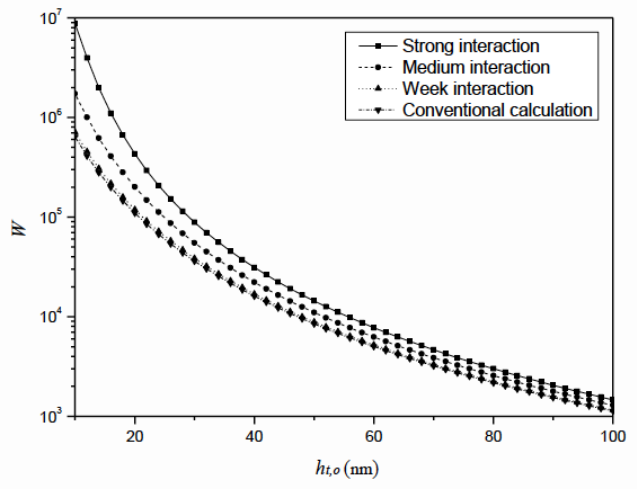

Figure 3: Variations with the outlet surface separation $h_{t,o}$ of the dimensionless load carried by the bearing for different fluid-bearing surface interactions and conventionally calculated when Δh=4nm and ψ=1.

Figure **4** shows that there is the optimum values of the bearing step size Δh which give the strongest multiscale effect for the medium and strong fluid-bearing surface interactions for given values of ψ and $h_{t,o}$. The value of Δh deviating from this optimum one alleviates the multiscale effect. When $h_{t,o}$=10nm, for the weak fluid-bearing surface interaction, the carried load of the bearing appears very close to the conventional calculation for all Δh values.

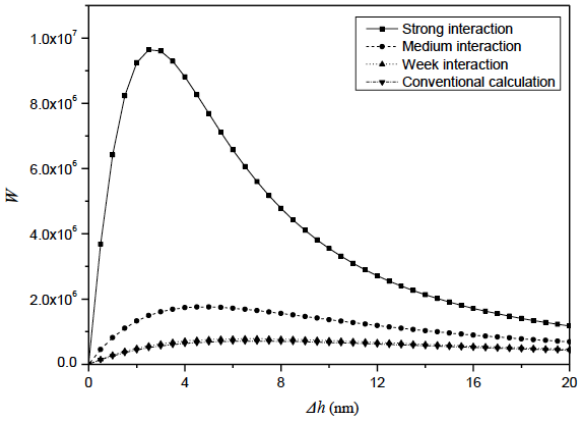

Figure 4: Variations with the bearing step size Δh of the dimensionless load carried by the bearing when ψ=1 and $h_{t,o}$=10nm.

Figure **5** shows that there is the optimum values of ψ, which are around 0.5, for the strongest multiscale effect for the medium and strong fluid-bearing surface interactions in the present bearing. The value of ψ deviating from this optimum one alleviates the multiscale effect. When $h_{t,o}$=10nm, for the weak fluid-bearing surface interaction, the carried load of the bearing appears very close to the conventional calculation for all ψ values.

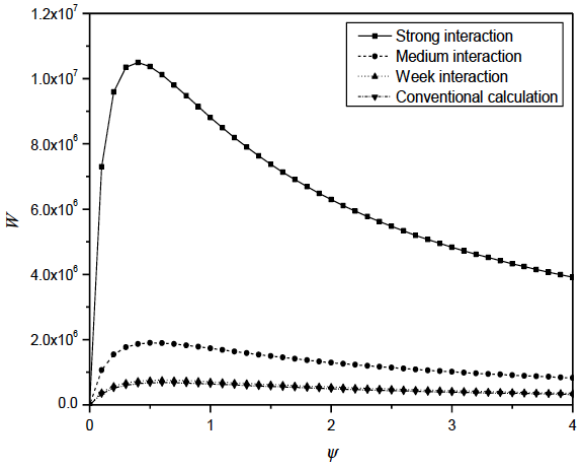

Figure 5: Variations with ψ of the dimensionless loads carried by the bearing respectively for different fluid-bearing surface interactions and conventionally calculated when Δh=4nm and $h_{t,o}$=10nm.

6. CONCLUSIONS

An analysis is presented for the multiscale hydrodynamics in the step bearing where simultaneously occur the adsorbed layer flow and the intermediate continuum fluid flow. The analysis used the flow factor approach model for nanoscale flow to describe the adsorbed layer flow and used the

Newtonian fluid model to describe the intermediate continuum fluid flow. The interfacial slippage on any interface was neglected. Based on the derived flow equations for the adsorbed layer and the intermediate continuum fluid, the explicit closed-form equations formulating the pressure distribution and the carried load of the bearing were obtained accounting for the multiscale hydrodynamic effect. Exemplary calculations were made respectively for the weak, medium and strong fluid-bearing surface interactions. The following conclusions are derived:

a) When the bearing surface separation is on the same scale with the thickness of the adsorbed layer, both the hydrodynamic pressure and the carried load of the bearing are greatly increased by the medium and strong fluid-bearing surface interactions owing to the adsorbed layer effect; However, the weak fluid-bearing surface interaction normally just has a slightly increasing effect.

b) For a wide outlet surface separation range, the significant multiscale effects were found for both the medium and strong fluid-bearing surface interactions, and they very pronouncedly increase the load-carrying capacity of the bearing. It shows that we may still not be able to conclude that the bearing has entered into the non-continuum lubrication regime according to the observation as there is a quite thick continuum fluid film lasting between the two adsorbed layers. The observed over high load-carrying capacity of the bearing may be just owing to the significant adsorbed layer effect.

c) There are the optimum values of the bearing step size Δh and the bearing geometrical parameter ψ for the strongest multiscale effect when the fluid-bearing surface interaction is medium or strong.

CONFLICT OF INTEREST

The authors declare that there is no conflict of interest with this research.

REFERENCES

[1] Pinkus O and Sternlicht B. Theory of hydrodynamic lubrication, McGraw-Hill, New York, 1961.

[2] Chan DYC and Horn RG. The drainage of thin liquid films between solid surfaces. Journal of Chemical Physics, 1985; 83: 5311-5324. https://doi.org/10.1063/1.449693

[3] Chauveteau G, Tirrell M and Omari A. Concentration dependence of the effective viscosity of polymer solutions in small pores with repulsive or attractive walls. Journal of Colloid and Interface Science 1984; 100: 41-54. https://doi.org/10.1016/0021-9797(84)90410-7

[4] Abraham FF. The interfacial density profile of a Lennard-Jones fluid in contact with a (100) Lennard-Jones wall and its relationship to idealized fluid/wall systems: A Monte Carlo simulation. Journal of Chemical Physics 1978; 68: 3713-3716. https://doi.org/10.1063/1.436229

[5] Bitsanis I, Vanderlick TK, Tirrell M and Davis HT. A tractable molecular theory of flow in strongly inhomogeneous fluids. Journal of Chemical Physics 1988; 89: 3152-3162. https://doi.org/10.1063/1.454972

[6] Atkas O and Aluru NR. A combined continuum/DSMC technique for multiscale analysis of microfluidic filters, Journal of Computational Physics 2002; 178: 342-372. https://doi.org/10.1006/jcph.2002.7030

[7] Liu J, Chen S, Nie X and Robbins MO. A continuum-atomistic simulation of heat transfer in micro- and nano- flows, Journal of Computational Physics 2007; 227: 279-291. https://doi.org/10.1016/j.jcp.2007.07.014

[8] Sun J, He Y and Tao WQ. Scale effect on flow and thermal boundaries in micro-/nano- channel flow using molecular dynamics-continuum hybrid simulation method, International Journal of Numerical Methods in Engineering 2010; 81: 207-228. https://doi.org/10.1002/nme.2683

[9] Yang X and Zheng ZC. Effects of channel scale on slip length of flow in micro/nano channels, ASME Journal of Fluids Engineering, 2010; 132: 061201. https://doi.org/10.1115/1.4001619

[10] Yen TH, Soong CY and Tzeng PY. Hybrid molecular dynamics-continuum simulation for nano/mesoscale channel flows, Microfluidics and Nanofluidics 2007; 3: 665-675. https://doi.org/10.1007/s10404-007-0154-7

[11] Zhang YB. The flow factor approach model for the fluid flow in a nano channel, International Journal of Heat and Mass Transfer 2015; 89: 733-742. https://doi.org/10.1016/j.ijheatmasstransfer.2015.05.092

[12] Zhang YB. Modeling of flow in a very small surface separation, Applied Mathematical Modeling 2020; 82: 573-586. https://doi.org/10.1016/j.apm.2020.01.069

[13] Zhang YB. Lubrication analysis for a line contact covering from boundary lubrication to hydrodynamic lubrication: Part I-Micro contact results, Journal of Computational and Theoretical Nanoscience 2014; 11: 62-70. https://doi.org/10.1166/jctn.2014.3318

Received on 05-12-2020 Accepted on 18-12-2020 Published on 29-12-2020

DOI: http://dx.doi.org/10.31875/2409-9848.2020.07.9